Supplementary Material : A Primary Radiation Standard Based on Quantum Nonlinear Optics

Samuel Lemieux,[1, *] Enno Giese,[2] Robert Fickler,[3] Maria V. Chekhova,[4, 5, 6] and Robert W. Boyd[1, 7]

[1]*Department of Physics and Max Planck Centre for Extreme and Quantum Photonics,*
University of Ottawa, 25 Templeton Street, Ottawa, Ontario K1N 6N5, Canada
[2]*Institut für Quantenphysik and Center for Integrated Quantum Science and Technology (IQST),*
Universität Ulm, Albert-Einstein-Allee 11, D-89081, Germany
[3]*Institute for Quantum Optics and Quantum Information (IQOQI),*
Austrian Academy of Sciences, Boltzmanngasse 3, 1090 Vienna, Austria
[4]*Max Planck Institute for the Science of Light, G.-Scharowsky Str.1/Bau 24, 91058 Erlangen, Germany*
[5]*Physics Department, Lomonosov Moscow State University, Moscow 119991, Russia*
[6]*University of Erlangen-Nuremberg, Staudtstrasse 7/B2, 91058 Erlangen, Germany*
[7]*Institute of Optics, University of Rochester, Rochester, New York 14627, USA*

We discuss several relevant quantities for radiometry in a general manner, in particular the connection of the photon statistics of a quantized mode to the number of photons detected by a detector. Further, we investigate the angular dependence of the intensity of down-converted light and the approximation used for angular mode selection by a pinhole and the wavelength dependence of the gain. Also, we describe the experimental setup in detail and discuss details of the data analysis for both the spontaneous and the high-gain regime of parametric down-conversion. We finally prove that the low-gain experiments have been performed in the spontaneous regime.

I. RADIOMETRY

Since the quantization of the electric field is usually performed in plane-wave modes denoted by a wave vector $\boldsymbol{k}$, we express general radiometric quantities through the photon number per plane wave mode $\mathcal{N}(\boldsymbol{k})$ of the field under consideration. A detector cannot detect all of these modes, and hence the detected photon-number density in the quantization volume can be written as

$$\varrho = \frac{1}{(2\pi)^3} \int_{\text{detector}} \mathrm{d}^3 k \, \mathcal{N}(\boldsymbol{k}) = \int_{\Delta\lambda} \mathrm{d}\lambda \int_{\Delta\Omega} \mathrm{d}\Omega \, \frac{1}{\lambda^4} \, \mathcal{N}(\boldsymbol{k}), \quad \text{(S1)}$$

where we used $\mathrm{d}^3 k = k^2 \mathrm{d}k \mathrm{d}\Omega = (2\pi)^3 \lambda^{-4} \mathrm{d}\lambda \mathrm{d}\Omega$ in the last step. We neglect here the index of refraction of air and assume that the detector has a bandwidth of $\Delta\lambda$ and collects light from a solid angle $\Delta\Omega$. In the following we introduce for a more convenient notation the Jacobian $\mathcal{D}(\lambda) = (2\pi)^3 \lambda^{-4}$, which is proportional to the mode density. For a sufficiently small detector bandwidth around the wavelength λ and a small solid angle around Ω, we can perform the integration and find

$$\varrho(\lambda, \Omega) \cong \frac{1}{(2\pi)^3} [\Delta\lambda \Delta\Omega] \mathcal{D}(\lambda) \mathcal{N}(\boldsymbol{k}), \quad \text{(S2)}$$

where $\mathcal{N}(\boldsymbol{k})$ implicitly depends on λ and Ω through the wave vector $\boldsymbol{k}$. This quantity is closely related to the spectral radiance $\hbar\omega(2\pi)^{-3}c\mathcal{D}(\lambda)\mathcal{N}$, which is the energy per units of time, area of the source, solid angle and bandwidth (in wavelength) of the detector [2].

To calculate the total number of photons that are detected, the density from eq. (S2) has to be integrated over the volume of the source,

$$N(\lambda, \Omega) = \int_{\text{source}} \mathrm{d}^3 r \, \varrho(\lambda, \Omega) \cong (2\pi)^{-3}[A_s c\tau_s][\Delta\lambda\Delta\Omega]\mathcal{D}\mathcal{N} \quad \text{(S3)}$$

where in the last step we assumed that the source has a surface area of A_s and emits light for a time duration τ_s.

We have not yet specified the photon distribution per plane wave mode $\mathcal{N}$. We do that in the next section and show that the assumption of a small solid angle as well as a small bandwidth of the detector is justified.

II. ANGULAR DISTRIBUTION OF SPONTANEOUS PDC

The photon statistics per plane wave mode $\mathcal{N}$ for spontaneous PDC of a bulk crystal of length L with a nonlinearity $\chi^{(2)}$ and illuminated by a plane wave pump with a field amplitude E_p is

$$\mathcal{N} = c^{-2} \left(L\chi^{(2)} E_p \right)^2 \frac{\omega_s}{n_s(\omega_s)} \frac{\omega_i}{n_i(\omega_i)} \operatorname{sinc}^2(\Delta\kappa L/2), \quad \text{(S4)}$$

where ω and ω_i are the frequencies of the signal and idler photons, and n_s and n_i their respective indices of refraction. The longitudinal wave vector mismatch $\Delta\kappa = k_p - \kappa_s - \kappa_i$ is the difference of the wave vector k_p of the pump and the longitudinal wave vectors $\kappa_{s,i} \equiv \sqrt{k_{s,i} - \boldsymbol{q}_{s,i}}$. Here, the signal and idler photons have the wave vectors k_s and k_i and the transverse wave vectors $\boldsymbol{q}_s$ and $\boldsymbol{q}_i$. Note that $k_j = \omega_j n_j/c$, with c the speed of light and ω_j the frequency of the signal, idler and pump fields with $j = s, i, p$.

* samzlemieux@gmail.com

With this notation, we find the expression

$$\Delta\kappa = k_p - k_s \left(\kappa_s/k_s + \sqrt{(k_i/k_s)^2 - (\boldsymbol{q}_i/k_s)^2} \right), \quad \text{(S5)}$$

for the longitudinal wave vector mismatch. Since we assume in (S4) a plane wave and monochromatic pump, we have due to energy conservation $\omega_i = \omega_p - \omega_s$ and due to momentum conservation $\boldsymbol{q}_s = -\boldsymbol{q}_i$. Hence, our expression depends only on ω_s and $\boldsymbol{q}_s$, which we can link to quantities of the detected field, which are written without a subscript. We find the connection $\omega_s = 2\pi c/\lambda$ when we express every quantity by the detected wavelength λ. Moreover, introducing spherical coordinates, we can define the polar angle θ of the detected field and have $\cos\theta = \kappa_s/k_s$ and $\sin\theta = \boldsymbol{q}_s/k_s$. The longitudinal wave vector mismatch

$$\Delta\kappa = k_p - k_s \left(\cos\theta + \sqrt{(k_i/k_s)^2 - \sin^2\theta} \right) \quad \text{(S6)}$$

therefore depends only on λ and θ, as does equation (S4).

In eq. (S2) we approximated the integral of $\mathcal{N}$ over $d\lambda$ and $d\Omega = \sin\theta d\theta d\phi$ by just multiplying the integration intervals. This is of course only valid if $\mathcal{N}$ depends weakly on both λ and θ over the range of interest.
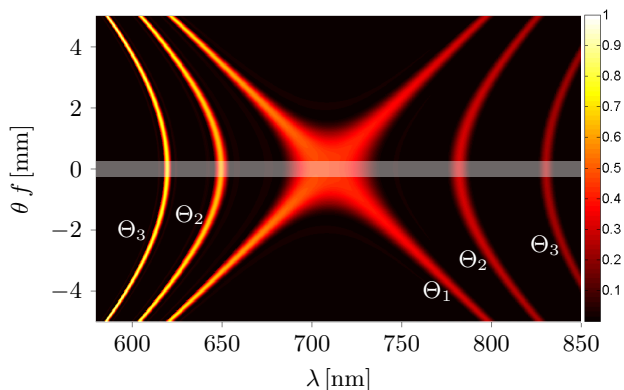

FIG. S1. Numerically generated spectrum of spontaneous PDC, plotting $\mathcal{D}(\lambda)\mathcal{N}$, for three different crystal tilt angles Θ, with Θ_1 corresponding to degenerate phase-matching in the emission angle $\theta = 0$. While $\mathcal{N}$ is the spectral density in the k-space, $\mathcal{D}(\lambda)\mathcal{N}$ corresponds to the spectral density in the angular-wavelength representation, which is the measurement basis of our spectrometer. The vertical axis is represented in terms of the position in the far-field, using a concave mirror of focal length $f = 200$ mm. The semi-transparent white strip is the angular filtering of a pinhole of size 0.5 mm positioned around $\theta = 0$.

In the experiment we place a pinhole in the far field of the spontaneous PDC light to filter a small range of angles. We show in the density plot of Fig. S1 the product $\mathcal{D}(\lambda)\mathcal{N}$ as a function of θ and λ and mark the size of our pinhole by a semi-transparent white strip. This numerical result is based on the Sellmeier equations of the three fields for BBO [3]. We further assume that $\mathcal{G}$ is constant

in the wavelength range of interest, and we justify this assumption in the next section. We work close to collinear propagation, with $\theta \approx 0$, where the function $\mathcal{D}(\lambda)\mathcal{N}$ does not vary significantly across the pinhole area so that we can perform the integration by just multiplying with the solid angle. Similarly, the size of a pixel corresponds roughly to a bandwidth of 0.063 nm. On this scale, the function $\mathcal{N}$ does not change significantly. Hence, our approximation in eq. (S2) is valid for our setup.

Of course, an integration of the pinhole angle can be performed as well to obtain an even more accurate result, but at some point the contribution of other crystal properties such as its length L as well as the dispersion relations of all the light fields will dominate. In the spirit of an easy-to-implement calibration technique, we refrained from this more complex analysis but emphasize that it is possible. In a similar manner, one could include both the frequency as well as the angular profile of the pump in eq. (S4). However, on axis this would not lead to a different result and our plane wave and monochromatic assumption is well-justified for our laser system.

III. WAVELENGTH DEPENDENCE OF GAIN

In the main body of our article, we assumed that the wavelength dependence of the gain function

$$\mathcal{G} = c^{-1}L\chi^{(2)}E_p/\sqrt{n_s n_i} \quad \text{(S7)}$$

can be neglected. In this section, we investigate different effects that could contribute to the wavelength dependence in our experiment and demonstrate that they do not vary much across the spectral region of interest. In addition to the linear dispersion ($n_s(\lambda)$ and $n_i(\lambda)$) as well as the nonlinear dispersion $\chi^{(2)}(\omega_p, \omega_s, \omega_i)$, obvious from eq. (S7), other contributions arise from tilting the angle of the crystal to scan different phase-matching conditions. By tilting the crystal, the Fresnel coefficients vary (for the pump or for the down-converted light) and the effective length L of the nonlinear crystal (defined as the length of propagation of the pump inside the crystal) changes. The different Fresnel coefficients change the intensity of the pump inside the crystal, as well as how much of the down-converted light couples out of the crystal. Using the Sellmeyer equations for BBO [3] and Miller's rule [1] (relating the first order and second order susceptibilities), we estimate the impact of those contributions, and show our results in Fig. S2. The largest deviations are attributed to the dispersion in the nonlinear susceptibility $\chi^{(2)}$ and to the change in the effective length of the nonlinear crystal upon tilting it. However, over a spectral range of 300 nm around degeneracy, the gain function $\mathcal{G}$ does not vary by more than 1%.
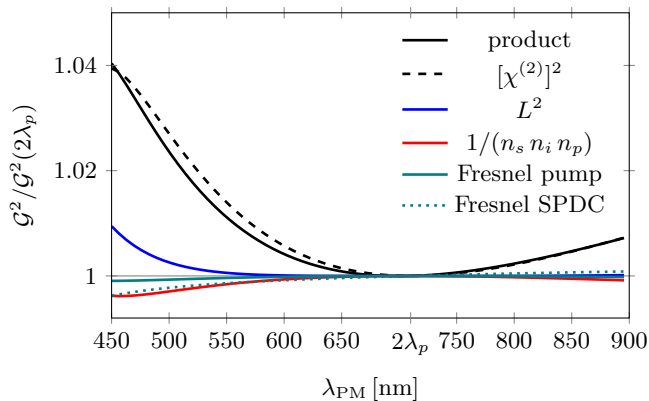
FIG. S2. Wavelength dependence of $\mathcal{G}^2$, normalized to its value at the degenerate frequency. Each phase-matched wavelength λ_{PM} corresponds to a set of refractive indices n_s, n_i and n_p (for the pump) that satisfy the phase-matching condition, occurring at a certain tilt of the nonlinear crystal. The refractive indices also influence the nonlinearity $\chi^{(2)}$, appearing as well in eq. (S7), through Miller's rule [1]. At a given energy per pulse, the electric field amplitude of the pump scales with n_p^{-1}. We combined this contribution with $1/(n_s n_i)$, which is explicit in the expression for $\mathcal{G}^2$. The varying angle between the pump propagation direction and the crystal leads to a different effective length L of the crystal. The Fresnel coefficients depend on the incidence angle and on the refractive indices: at the entrance facet the coefficients change how much of the pump E_p is transmitted into the nonlinear medium; the exit facet changes the amount down-converted light that couples out. The solid black line is the product all these effects.
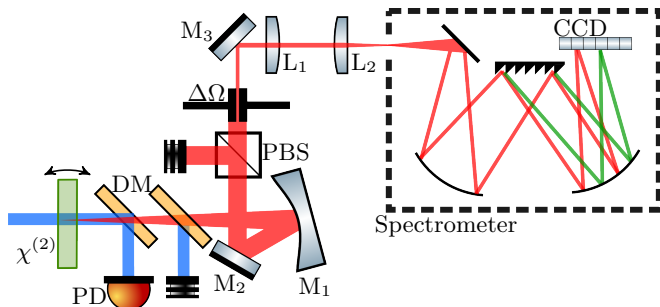

FIG. S3. Experimental setup. The down-converted light from the nonlinear crystal $\chi^{(2)}$ is angularly filtered in the far field by the pinhole $\Delta\Omega$. The plane of the pinhole is then imaged onto the entrance of the imaging spectrograph, which brings the grating-diffracted light onto the CCD camera.

IV. EXPERIMENTAL SETUP

The third harmonic (355 nm wavelength, 29.4 ps pulse duration, 50 Hz repetition rate) of a pulsed Nd:YAG laser is prepared to serve as the pump for PDC: a pair of dispersive prisms suppresses the spurious frequencies from the laser; a half-wave plate and α-BBO Glan-Laser polarizer set the polarization; a pair of lenses (focal lengths $f_1 = 300$ mm and $f_2 = 100$ mm, separated by the dis-

tance $f_1 + f_2$) bring the diameter of the laser beam down to approximately 0.6 mm; a pinhole of size 100 µm is introduced between the lenses at the beam focus (distance f_1 from the first lens) to spatially filter the beam; and another α-BBO Glan-Laser polarizer confirms the polarization of the beam.

The remainder of the experimental setup is shown in Fig. S3. Parametric down-conversion is generated from the interaction of the pump beam with a nonlinear crystal $\chi^{(2)}$ (β-BBO, 3-mm thickness, type-I phase-matching, uncoated, cut for degenerate PDC with a 355-nm pump) on a motorized rotation mount. The wavelengths that satisfy the phase-matching condition are tuned by varying the angle between the optic axis of the crystal and the wavevector of the pump. Two dichroic mirrors (DM) suppress the pump after the crystal and reflect the pump light onto a photodiode (PD) to monitor its intensity. A concave mirror (M$_1$) of focal length 200 mm is used to bring the down-converted light to the far field, where a pinhole $\Delta\Omega$ (0.5 mm diameter) selects a small solid angle. A broadband polarizing beam spliter PBS placed before the iris is set to transmit the polarization of the down-converted light. A pair of lenses of (L$_1$) and (L$_2$) of focal lengths 200 mm and 150 mm are used to image the iris onto the entrance slit (1-mm wide) of the spectrometer, with a magnification of $4/3$. The spectrometer is an imaging spectrograph (Acton SP-2558) with a CCD camera (PIXIS:100BR_eXcelon, 1340×100 pixels of size $20\,\mu\mathrm{m} \times 20\,\mu\mathrm{m}$). The integration time for each spectrum is 500 ms. Transverse hardware binning (summing the photoelectron count for the 100 transverse pixels) is enabled. Each spectrum spans the range from 450 nm to 900 nm. To cover this range, we need to repeat the acquisition for different angular positions of the grating (600 grooves per mm, 500-nm blaze). The experiment is automated: after each acquisition by the spectrometer, the motorized holder rotates the crystal through an angle of about 0.01°, up to a total change of approximately 8°. The pump energy measured at the photo-diode is recorded for each position of the crystal. The wavelength of the spectrometer is calibrated using a neon-argon lamp along with Princeton Instruments Intellical system. After the experiment a reference lamp is introduced at the crystal plane. Its spectrum is acquired using the same experimental settings. The reference response function that we use to verify our method is obtained by comparing the measured spectrum of a calibration lamp (LED-stack with a diffuser for relative intensity calibration) and a reference spectrum provided by Princeton Instruments.

V. DETAILS ON THE DATA ANALYSIS

Our calibration method relies on the comparison of the measured phase-matched number of counts $M(\lambda_{\mathrm{PM}})$ to the expected number of phase-matched photons $N(\lambda_{\mathrm{PM}})$. We therefore acquire a large number of spectra M_j corresponding to different phase-matching conditions over

a broad spectral range. However, the peak number of counts in a measured spectrum does not correspond, in general, to $M(\lambda_{\text{PM}})$. Instead, we can extract the response function from the properties of $\mathcal{N}$. From the main text, we know that

$$\mathcal{N} \sim \omega(\omega_p - \omega) \operatorname{sinc}^2(\Delta\kappa L/2) \leq \omega(\omega_p - \omega), \quad \text{(S8)}$$

where the inequality becomes equality only for phase matching $\Delta\kappa = 0$. We denote the wavelength of phase matching with λ_{PM}. With eq. (5) from the main text we find the inequality

$$R(\lambda) \geq R(\lambda) \operatorname{sinc}^2 \frac{\Delta\kappa L}{2} \propto \frac{M_j(\lambda)}{\mathcal{D}(\lambda)\omega(\omega_p - \omega)} \quad \text{(S9)}$$

with an equality sign for $\lambda = \lambda_{\text{PM}}$. If we approximate the phase matching function by a Gaussian, i.e.,

$$\operatorname{sinc}^2(\Delta\kappa L/2) \propto \exp[-(\lambda - \lambda_{\text{PM}})^2/(2\sigma_\lambda^2)], \quad \text{(S10)}$$

it is easy to show that the peak of the product $R(\lambda) \operatorname{sinc}^2(\Delta\kappa L/2)$ shifts to the wavelength

$$\tilde{\lambda} = \lambda_{\text{PM}} + \frac{1}{R}\frac{\mathrm{d}R}{\mathrm{d}\lambda}\bigg|_{\tilde{\lambda}} \sigma_\lambda^2. \quad \text{(S11)}$$

Hence, the shift between phase-matched wavelength and peak increases, the steeper the slope of the response function or the wider the peak is. Since the response function is not known but is the result of the calibration procedure, eq. (S11) cannot be used to determine the phase-matching wavelength. However, eq. (S9) directly gives a method to determine the response function despite the shift: when we acquire a large number of spectra M_j, each with a slightly varying λ_{PM}, the amplitude of $M_j/[\mathcal{D}\omega(\omega_p - \omega)]$ at one particular wavelength is the largest if the wavelength corresponds to λ_{PM}. Hence, we obtain the response function from

$$R(\lambda) = \max_j \left[\frac{M_j(\lambda)}{\mathcal{D}(\lambda)\omega(\omega_p - \omega)} \right] \bigg/ \max_j \left[\frac{4M_j(2\lambda_p)}{\mathcal{D}(2\lambda_p)\,\omega_p^2} \right], \quad \text{(S12)}$$

where we normalize the response function to unity at the degenerate wavelength $\lambda = 2\lambda_p$. To reduce errors in the analysis according to eq. (S12), we suppress for each $M_j(\lambda)$ spectrum the high-frequency content, filtered out via a fast-Fourier-transform procedure.

A similar idea can be used for absolute calibration. For an arbitrary $\mathcal{G}$, the photon distribution per plane-wave mode assuming a monochromatic plane wave pump can be written as [4]

$$\mathcal{N}^{(\text{HG})} = \frac{\mathcal{G}^2\mathcal{Q}^2}{\mathcal{G}^2\mathcal{Q}^2 - (\Delta\kappa L/2)^2} \sinh^2 \sqrt{\mathcal{G}^2\mathcal{Q}^2 - (\Delta\kappa L/2)^2}, \quad \text{(S13)}$$

where $\mathcal{Q}^2 \equiv \omega(\omega_p - \omega)$, and the superscript (HG) highlights that we are using this equation to describe the high-gain regime of PDC. Since the maximum of this function occurs for phase matching ($\Delta\kappa = 0$), we find

$$\mathcal{N}^{(\text{HG})} \leq \sinh^2(\mathcal{G}\mathcal{Q}) \equiv \mathcal{N}_{\text{PM}}^{(\text{HG})} \quad \text{(S14)}$$

where we defined the phase-matched photon distribution $\mathcal{N}_{\text{PM}}^{(\text{HG})}$ that has the well-known hyperbolic form of parametric amplification and is used in the main body of our article. Note further that for $\mathcal{G}\mathcal{Q} \ll 1$ we recover the low-gain result.

The quantum efficiency at the degenerate wavelength $\alpha = \eta(2\lambda_p)$ is

$$\alpha = M_j(\lambda)/[R(\lambda)N(\lambda)] \quad \text{(S15)}$$

with the definitions from the main body of the article. With that, we find from eq. (S14) and with the help of eq. (S3) the inequality

$$\alpha \sinh^2 \mathcal{G}\mathcal{Q} \geq M_j(\lambda)/[R(\lambda)\mathcal{D}(\lambda)\Delta\Omega\Delta\lambda A_s c\tau_s], \quad \text{(S16)}$$

where again the equal sign is valid for $\lambda = \lambda_{\text{PM}}$. Hence, we find, similarly to the low-gain method,

$$\alpha \sinh^2 \mathcal{G}\mathcal{Q} = \max_j \left[\frac{M_j(\lambda)}{R(\lambda)\mathcal{D}(\lambda)\Delta\Omega\Delta\lambda A_s c\tau_s} \right] \quad \text{(S17)}$$

as an exact equality if the spectra are sufficiently dense. Taking the maximum of all recorded spectra, each one of them divided by $R(\lambda)\mathcal{D}(\lambda)$ and a numerical factor that depends on laboratory parameters (spatial dimensions and bandwidths), we can fit the data to the function $\alpha \sinh^2 \mathcal{G}\mathcal{Q}$ with two fitting parameters α and $\mathcal{G}$. Note that we do not need to measure the exponential increase of the generated photons with increasing pump intensity, but determine both parameters from the distortion of the *spectral shape* of the maximum of all spectra. With this fitting procedure, one can not only determine the quantum efficiency $\eta(\lambda) = \alpha R(\lambda)$, but also the gain $\mathcal{G}$.

Even though we do not use the exponential increase with the pump power for our calibration method, we still record the intensity while scanning different phase matching functions. We do this to correct for drifts and fluctuations during the course of one measurement. We are then able to perform the fitting procedure using $\mathcal{G}/E_j$, where E_j is the pump field amplitude during measurement corresponding to the the jth phase-matching condition.

The α obtained using our method for absolute calibration is compared to an estimated quantum efficiency based on the properties of each optical component in the experimental setup, listed in table I. The efficiency of uncoated components is estimated from the Fresnel coefficients, while the efficiency of coated components is taken from the manufacturers.

VI. SPONTANEOUS REGIME OF PARAMETRIC DOWN-CONVERSION

As shown in the section above in eq. (S13), the photon-number distribution grows exponentially with the intensity of the pump. In the low-gain regime, where the photon pairs are generated spontaneously, the number

TABLE I. Contribution of each optical component to the total quantum efficiency of the experimental setup. The parentheses denote the number of components. The total efficiency is obtained by multiplying all the contributions and propagating the uncertainties accordingly.

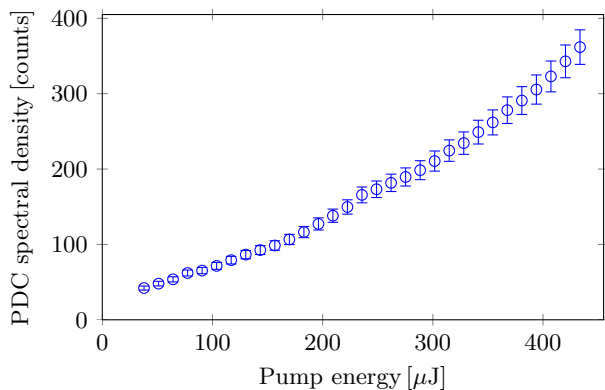| Optical component	Efficiency
Crystal output facet (1)	0.94 ± 0.01
Dichroic mirror (2)	0.95 ± 0.01
Dielectric mirrors (6)	0.99 ± 0.01
Polarizing beam splitter (1)	0.98 ± 0.01
Uncoated lens (2)	0.92 ± 0.01
Diffraction grating (1)	0.60 ± 0.02
Spectrometer camera (1)	0.95 ± 0.02
Total	0.38 ± 0.07

FIG. S4.   PDC spectral density as a function of the pump energy per pulse. The number of counts was extracted at the phase-matched wavelength $\lambda = 690$ nm. The error bars are obtained from the amplitude of the noise in the spectrum. The acquisition time is 5 seconds, for a total of 250 pulses.

of photons grows linearly with the intensity which can be seen from the expansion

$$\mathcal{N}_{\mathrm{PM}}^{(\mathrm{HG})} = \sinh^2 \mathcal{G}\mathcal{Q} \cong \mathcal{G}^2\mathcal{Q}^2 = \mathcal{G}^2\omega(\omega_p - \omega) = \mathcal{N}_{\mathrm{PM}}, \tag{S18}$$

where $\mathcal{N}_{\mathrm{PM}}$ is the low-gain photon distribution for phase matching. To obtain the response function $R(\lambda)$, we do not need to know the exact value of $\mathcal{G}$ but rely on the fact that the first-order expansion above is valid. Note that $\mathcal{G}^2$ is proportional to the intensity of the pump I_p [4]. To verify that we work in the spontaneous regime of PDC, we measure the number of counts for a single wavelength and increase the pump intensity. The results are shown in Fig. S4. We see, that we are well in the linear regime up to roughly 150 µJ. We performed the relative calibration experiment at a pump intensity of 100 µJ, while the high-gain part of the experiment used a more intense pump, around 200 µJ and higher.

[1] Boyd, R. W. *Nonlinear optics* (Academic Press, 2003).
[2] Datla, R. U. & Parr, A. C. 1. introduction to optical radiometry. *Optical Radiometry. Series: Experimental Methods in the Physical Sciences, ISBN: 9780124759886. Elsevier, vol. 41, pp. 1-34* **41**, 1–34 (2005).
[3] Eimerl, D., Davis, L., Velsko, S., Graham, E. K. & Zalkin, A. Optical, mechanical, and thermal properties of barium borate. *Journal of Applied Physics* **62**, 1968–1983 (1987).
[4] Klyshko, D. N. *Photons and Nonlinear Optics* (Gordon and Breach, 1989).